Compatibility between Activity and Selectivity in Catalytic Oxidation of Benzyl Alcohol with Au-Pd Nanoparticle through Redox Switching of SnO x

Pingping Wu, Zhengke He, Yonghui Liu, Lei Song, Chunzheng Wang, Edgar Muhumuza, Peng Bai, Lianming Zhao, Svetlana Mintova, Zifeng Yan

Compatibility between Activity and Selectivity in Catalytic Oxidation of Benzyl Alcohol with Au-Pd Nanoparticle through Redox Switching of SnO_x

Pingping Wu,[‡] *Zhengke He,*[‡] *Yonghui Liu,*[#] *Lei Song,*[‡] *Chunzheng Wang,*[‡] *Edgar Muhumuza,*[‡] *Peng Bai,*[‡,]* *Lianming Zhao,*[#,]* *Svetlana Mintova,*[‖] *Zifeng Yan*[‡]

[‡]State Key Laboratory of Heavy Oil Processing, CNPC Key Laboratory of Catalysis, College of Chemical Engineering, China University of Petroleum (East China), Qingdao 266580, China

[#]School of Materials Science and Engineering, Institute of Advanced Materials, China University of Petroleum (East China), Qingdao, 266580, China

[‖]Normandie University, ENSICAEN, UNICAEN, CNRS, Laboratoire Catalyse et Spectrochimie, 14000 Caen, France

ABSTRACT: A balance between the catalytic activity and product selectivity remains a dilemma for the partial oxidation processes because the products are prone to be over-oxidized. In this work we report on the partial oxidation of benzyl alcohol using a modified catalyst consisting of nanosized Au-Pd particles (NP) with tin oxide (SnO_x) deposited on mesoporous silica support. We found that the SnO_x promotes the autogenous reduction of PdO to active Pd^0 species on the Au-Pd NP catalyst (SnO_x@AP-ox) before H_2 reduction, which is due to the high oxophilicity of Sn. The presence of active Pd^0 species and the enhancement of oxygen transfer by SnO_x led to a high catalytic activity. The benzaldehyde selectivity was enhanced with the increase of SnO_x content on catalyst SnO_x@AP-ox, which is ascribed to the modulated affinity of reactants and products on the catalyst surface through the redox switching of Sn species. After H_2 reduction, the SnO_x was partially reduced and Au-Pd-Sn alloy was formed. The formation of Au-Pd-Sn alloy weakened both the catalytic synergy of Au-Pd alloy NPs and the adsorption of benzyl alcohol on the reduced catalyst, thus leading to a low catalytic activity.

KEYWORDS: SnO_x, Au-Pd, oxygen transfer, alloying, benzyl alcohol oxidation

1. INTRODUCTION

The catalytic partial oxidation to produce various fine chemicals is a vital research area for the pharmaceutical, food, and cosmetic industries.[1] One of such processes in the modern synthetic chemical industry is the catalytic partial oxidation of primary alcohols to their corresponding intermediates,[2] such as benzyl alcohol oxidation to

benzaldehyde, benzyl benzoate, benzoic acid and/or benzyl ether depending on the catalytic system and reaction conditions used.[3-4] Among which benzaldehyde is considered as the most valuable product and widely used in the manufacture of flavors, pharmaceuticals, dyes, spices, etc.[5] Oxidizing a primary alcohol to an aldehyde using molecular oxygen/air as an oxidant conforms with the principles of green and sustainable chemical processes since water is the only by-product.[1] However, the desired products are highly reactive and susceptible to over oxidization generating low-value by-products, which results in low product selectivity during selective oxidation with oxygen/air as oxidant. In the industrial process, high product selectivity is generally achieved through the control of conversion, which results in low single-pass conversion, excessive recovery of unreacted reactant and high energy consumption. Therefore, it has been a long-standing dilemma between the high activity and high selectivity for the partial oxidation catalysts.

Au-Pd bimetallic catalysts are the most frequently reported for benzyl alcohol partial oxidation;[6-8] and a catalytic synergy between these two metals has been observed. This catalytic synergy was attributed to the formation of Au–Pd alloy NPs and electrons transfer between surface Au and Pd atoms, preventing the formation of inert surface PdO species.[8-10] Metallic Pd^0-enriched clusters/surface has been reported as active sites for O_2 activation,[8-14] however, Pd-enriched surfaces are usually coated with a layer of inert PdO.[15-16] This contradictive condition has been improved to a certain extent by introducing Au to Pd with H_2 reduction process. Electrons rearrangement between Au and Pd atoms facilitates the formation of metallic

Pd^0-enriched clusters/surface on H_2 reduced Au-Pd bimetallic NP catalyst.[16-17] However, Wiley and co-workers observed a surface enrichment of Au on Au-Pd alloy NPs after H_2 reduction, resulting in a decrease of Pd^0-enriched surface-active sites.[16] These results pointed out to the need to find another route to reduce the surface inert PdO layers on Au-Pd NP catalyst. Pd has a relative high electron negativity and a low oxygen affinity,[17-18] while Sn is considered as an oxophilic metal.[17, 19-20] Thus, this reminds us to consider the possibility of applying tin as a potential promoter for in-situ autogenous reduction of surface PdO layer instead of high temperature H_2 reduction.

Meanwhile as we mentioned above, the dilemma between the high activity and high selectivity for benzyl alcohol partial oxidation also persists on Au-Pd bimetallic NP catalyst. A high benzyl alcohol conversion (> 90%) was obtained on Au-Pd bimetallic catalysts but with a relative low benzaldehyde selectivity of 50% ~ 60%.[8] Studies have shown that the introduction of auxiliaries can regulate the surface affinity to reactants, products or intermediates to reduce side reactions and improve product selectivity.[13, 21-22] He et al. demonstrated that when a small amount of Pt metal was alloyed with Au-Pd sol, a high selectivity to benzaldehyde was achieved on the solvent-free oxidation of benzyl alcohol.[1] Hutchings et al. applied SnO_x promoted Pd/TiO_2 catalyst for hydrogen peroxide synthesis.[13] The promoted catalyst exhibited high H_2O_2 selectivity attributable to the presence of the SnO_x surface layer which prevented further hydrogenation and decomposition of H_2O_2. In our previous work,[23] we found that applying SnO_x promoted Au nanoparticle (NP) catalyst for benzyl

alcohol oxidation can effectively reduce the disproportionation reaction, achieving a high benzaldehyde selectivity. In summary, tin is a potential promoter for in-situ reduction of surface PdO species because it is more oxophilic and it can also effectively enhance the benzaldehyde selectivity on Au NP catalyst by regulating the surface affinity.[23]

In this paper we report the preparation of Au-Pd bimetallic NP catalyst modified with Sn/SnO_x. First, the mesostructured cellular foam silica (MCF) supported Au-Pd NP catalyst (AP-ox) was prepared by a one-pot method.[8] Second, the SnO_x was deposited on the surface of Au-Pd NPs to obtain the SnO_x@AP-ox catalysts. The results showed that the SnOx significantly enhanced the benzaldehyde yield thus broking the dilemma between the high activity and high selectivity of Au-Pd NPs catalyst. The role of SnO_x in modulating the catalyst performance was approved experimentally and theoretically.

2. EXPERIMENTAL SECTION

2.1. Chemicals. $HAuCl_4 \cdot xH_2O$ (Sinopharm Chemical), $PdCl_2$ (Sinopharm Chemical), $SnCl_2 \cdot H_2O$ (Sinopharm Chemical), tetraethyl orthosilicate (TEOS, 98%, Sinopharm Chemical), triblock co-polymer $PEO_{20}PPO_{70}PEO_{20}$ (P123, Aldrich), mercaptopropyltrimethoxysilane (MPTMS, 97%, Aldrich), 1,3,5-trimethylbenzene (99%, Sinopharm Chemical), hydrochloric acid (37%, Sinopharm Chemical), benzyl alcohol (99.99%, Sinopharm Chemical), benzaldehyde (99.99%, Sinopharm Chemical), benzoic acid (99.99%, Sinopharm Chemical) and absolute ethanol (99.98%, Sinopharm Chemical) were used as received without further purification.

2.2. Preparation of Unmodified Catalysts. Supported Au-Pd NP catalyst was prepared following the procedure reported in our previous work.[8] In a typical synthesis, 8.0 g of P123 was dissolved in 60 mL deionized water, followed by introduction of 20 mL of concentrated hydrochloric acid (37%) at room temperature. Then, 8 g of 1,3,5-trimethylbenzene was added into the clear solution as a pore swelling agent and stirred at 38 ^{o}C for 2 h, followed by the dropwise addition of 18.4 g TEOS and 1.14 g MPTMS into the mixture. Finally, the $HAuCl_4$ and $PdCl_2$ solutions were added into the synthesis mixtures. After stirring at 38 ^{o}C for 24 h, the mixtures were transferred to a Teflon-lined stainless-steel autoclave to undergo a hydrothermal treatment at 100 ^{o}C for 24 h. The obtained solids were purified with deionized water, dried at 80 ^{o}C overnight, and eventually calcined in air at 550 ^{o}C for 6 h to remove the templating and coupling agent. Catalysts with a total noble metal (Au + Pd) loading of 0.75 wt.% with an Au loading of 0.25 wt.% and a Pd loading of 0.5 wt.% were abbreviated as AP-ox and the reduced samples were denoted as AP-H_2. Monometallic catalysts Au-ox with an Au weight ratio of 0.25% and Pd-ox with a Pd weight ratio of 0.5% were prepared as references. The catalysts 2Pd-ox with a Pd weight ratio of 1.0% and 2AP-ox with Pd and Au weight ratio of 1.0%, respectively, were also prepared for comparison purpose.

2.2.1 Preparation of SnO_x@AP Catalysts. 2 g of AP-ox solid was dispersed in a stannous chloride solution and stirred at room temperature for 4 h until a slurry was formed. The obtained slurry was dried at 100 ^{o}C for 12 h and finally calcined at 300 ^{o}C for 4 h under air atmosphere. Different amounts of SnO_x were introduced and the

obtained catalysts were denoted as ySnO$_x$@AP-ox (y represents the nominal weight percentage of SnO$_x$, such as 0%, 0.2%, 0.5%, 1.0%, x=1 ~ 2). These catalysts were reduced at 300 ^{o}C for 2 h under H_2 atmosphere to investigate the effect of reduction on the catalytic performance; the obtained catalysts were denoted as ySnO$_x$@AP-H_2.

For comparison, catalysts 1%SnO$_x$@2Pd-ox and 1%SnO$_x$@2AP-ox with higher noble metal loadings were prepared following the same procedure and reduced under H_2 atmosphere to obtain samples 1%SnO$_x$@2Pd-H_2 and 1%SnO$_x$@2AP-H_2, respectively.

2.3 Characterization. N_2 adsorption/desorption was carried out to analyze the textural properties of catalysts after degassing at 300 ^{o}C for 4 h under vacuum using an automatic volumetric sorption analyzer (Micromeritics, TriStar 3000). X-ray powder diffraction (XRD) patterns of catalysts were recorded on a X'Pert PRO MPD system (Dutch company Panaco) with a Cu $K\alpha$ radiation (λ = 0.15418 nm) at 35 kV and 40 mA. High angle annular dark field (HAADF) images and X-ray energy dispersive spectroscopy (XEDS) of the catalysts were obtained using a scanning transmission electron microscope (STEM) (JEOL JEM-2100F) with an acceleration voltage of 200 kV. HAADF images of nanoparticles were collected on HITACHI HF5000 field emission transmission electron microscope equipped with a spherical aberration corrector (AC-TEM) and energy dispersive spectroscopy (EDS) from Oxford operated at 200 kV. Actual noble metal loadings in the catalysts were determined by inductively coupled plasma optical emission spectroscopy (ICP-OES) using a VISTA-MPX Varian system. The solid ultraviolet-visible (UV-vis) spectra of

catalysts were collected by a Hitachi U-4100 UV-vis-NIR spectrophotometer using $BaSO_4$ as an internal reference. The diffuse reflectance spectra from 350 to 800 nm were recorded. The surface chemical properties of the catalysts were analyzed using a K-alpha X-ray spectrometer (XPS) manufactured by Thermo Fisher Scientific. Taking the Al electrode as the anode, the electron kinetic energy was 1486.6 eV. The spectra were calibrated with C1s binding energy (284.5 eV) as a calibration binding energy (BE) reference. In situ diffuse reflectance infrared Fourier transform spectroscopy (DRIFTS) of CO adsorption on the fresh catalysts (pretreated in H_2 at 573 K at a flow rate of 20 mL min^{-1} for 60 min, cooled down to 303 K and purged with He for 30 min) was conducted in a high-temperature diffuse reflection reaction cell (PIKE). The spectra were recorded on a BRUKER VERTEX70V FT-IR spectrometer at room temperature with a resolution of 4 cm^{-1}. H_2-temperature programmed reduction (H_2-TPR) experiments were conducted on a chemisorption apparatus (Micromeritics AutoChem II 2920). Typically, the sample (100 mg) was pre-treated at 300 °C for 1 h under an Ar stream (30 mL/min). Afterwards, the system was cooled to 50 °C, and then a 10 vol% H_2/Ar stream (30 mL/min) was introduced. The temperature was raised linearly from 100 °C to 800 °C at a rate of 10 °C/min, and the signal was recorded by a thermal conductivity detector (TCD).

2.4 Selective Oxidation of Benzyl Alcohol. The selective oxidation of benzyl alcohol was carried out in a 100 mL autoclave with a polytetrafluoroethylene liner (Model: SLM100, Beijing Easychem Science and Technology Development Company, China). Typically, 10.8 g of benzyl alcohol and 50 mg of solid catalyst

were charged into the reaction vessel. After purging with O_2 for 3 times, the temperature was raised to 110 ^oC and the O_2 pressure was maintained at 0.8 MPa for 2 h under stirring. Then, the products were separated and analyzed using a gas chromatograph (Agilent 6870) equipped with a FID detector and a DB-1 column (30*0.32*0.25). The turnover frequency (TOF) was calculated based on the moles of benzyl alcohol converted per mole of noble metals (Au + Pd) per hour.

2.5 Theoretical Calculation. The spin-polarized density functional theory (DFT) calculations were implemented using the DMol^3 program of Materials Studio 2018 software package.[24-25] The exchange-correlation term was described within the general gradient approximation developed by Perdew, Burke, and Ernzerhof (GGA−PBE).[26] Particularly, Grimme's PBE+D2 method was used to correct the long-range dispersion forces,[27] which shows a comparable reliability with the PBE0 hybrid XC functional including an ab initio Van der Waals correction.[28] The ion cores of metal atoms were treated with the density functional semicore pseudopotential (DSPP), while the valence electron functions were represented by the localized double-numerical basis with polarization (DNP) function. The transition state structures were located by using the linear synchronous transition/quadratic synchronous transit method,[29] confirmed by the frequency calculations. A real-space global orbital cutoff of 4.9 Å was adopted to keep the balance between high quality of results and high computational cost. The convergence tolerances for energy change, max force, and displacement were 1×10^{-5} Ha, 2×10^{-3} Ha $Å^{-1}$, and 5×10^{-3} Å, respectively. According to the experimental results, a homogeneous Pd_3Au alloy with

a Pd-Au atomic ratio of 3:1 was selected as the palladium-gold alloy model, and a stable close-packed (111) surface was chosen as the model surface ($Pd_3Au(111)$). The $Pd_3Au(111)$ model was established by a four-layers periodic slab model with a p(4×4) unit cell and a vacuum region of 15 Å. The $Pd_3Sn_3Au(111)$ model was created by replacing the Pd atoms on the top surface layer of $Pd_3Au(111)$ with Sn atoms in a ratio of 1:1, and the other bottom three layers still maintained as Pd_3Au. The $Pd_3Au(111)$ surface was covered by a layer of Sn, SnO, and SnO_2 species to form $Sn/Pd_3Au(111)$, $SnO/Pd_3Au(111)$, $SnO_2/Pd_3Au(111)$ models, respectively. Sn, SnO, and SnO_2 species were doped on the $Pd_3Au(111)$ surface to form $Sn/Pd_3Au(111)$, $SnO/Pd_3Au(111)$, $SnO_2/Pd_3Au(111)$ models, respectively. In $Sn/Pd_3Au(111)$, $SnO/Pd_3Au(111)$, $SnO_2/Pd_3Au(111)$, the number of Sn, SnO, and SnO_2 units was half of the atom number of the top-layer $Pd_3Au(111)$, where the unit cell contained 8 Sn, SnO, and SnO_2 units, respectively. In the slab calculations, the atoms in the two bottom layers were fixed in their bulk positions, but all other atoms were allowed to be fully relaxed.

The adsorption energy (E_{ads}) of an adsorbate on catalyst surfaces was defined as

$$E_{ads} = E_{adsorbate/substrate} - (E_{adsorbate} + E_{substrate}),$$

where $E_{adsorbate/substrate}$ and $E_{substrate}$ correspond to the total energy of the catalyst substrate with and without an adsorbed molecule, respectively, while $E_{adsorbate}$ represents the energy of the free adsorbate.

3. RESULTS AND DISCUSSION

3.1 Catalyst Characterization. N_2 adsorption-desorption isotherms and pore size distribution curves of catalysts *y*SnO_x@AP-ox(H_2) are shown in Figure S1A, B and the results are summarized in Table 1. A typical type IV isotherm was measured on all catalysts, which contains a H-2 hysteresis loop, indicating an ink-bottle mesoporous structure. Reference catalysts Pd-ox and AP-ox exhibited a high specific surface area ($\sim$ 800 m^2/g) and a large pore volume (1.8 $\sim$ 2.3 cm^3/g). A small amount of SnO_x introduced in catalysts 0.2%SnO_x@AP-ox and 0.5%SnO_x@AP-ox leads to a slight decrease of the specific surface area (700 - 750 m^2/g). While the specific surface area of catalyst 1.0%SnO_x@AP-ox significantly decreases to $\sim$ 650 m^2/g when 1wt.% of SnO_x was added. The average pore diameter increased from 5.6 nm for catalyst 0.2%SnO_x@AP-ox to 7.8 nm for catalyst 1.0%SnO_x@AP-ox. The decrease of specific surface area and pore volume on catalyst 1.0%SnO_x@AP-ox was attributed to the partial blocking of small pores after introducing a relatively large amount of SnO_x.

Table 1. Physical Properties of Catalysts.

Catalysts	Metal loading [a] (*wt.*%)			S_{BET} (m^2/g)	Pore volume (cm^3/g)	Pore diameter (nm)
	Au	Pd	Sn			
Pd -ox	0	0.5	0	839	1.8	5.7
AP-ox	0.25	0.49	0	791	2.3	9.6
0.2%SnO_x@AP-ox	0.24	0.50	0.18	698	1.6	5.6
0.5%SnO_x@AP-ox	0.24	0.49	0.44	747	1.7	5.6
1.0%SnO_x@AP-ox	0.25	0.49	0.88	650	1.6	7.8
0.5%SnO_x@AP-H_2	0.24	0.48	0.44	653	1.6	5.6

[a] The metal loading was evaluated by ICP-OES. S_{BET}, surface area calculated by the BET method.

V_{total}, total pore volume calculated at P/P_o = 0.998. Pore diameter calculated from the adsorption branch using BJH method.

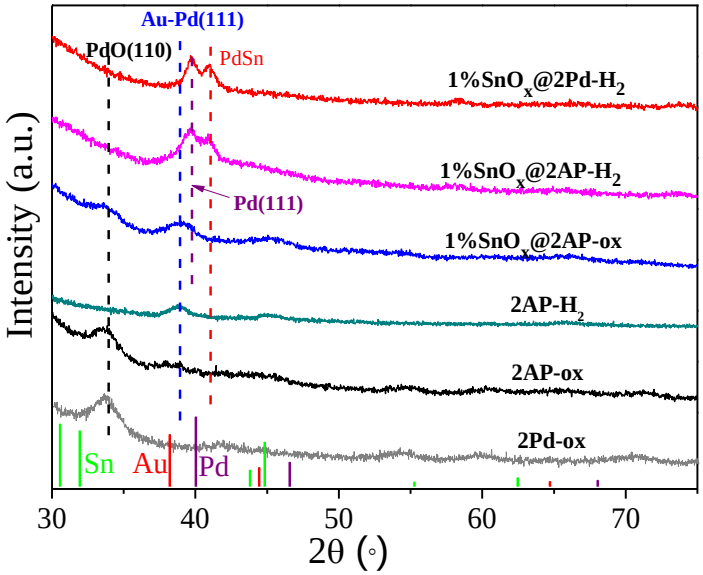

Figure 1. XRD patterns of catalysts 2Pd-ox, 2AP-ox, 2AP-H_2, *1%*SnO_x@2Pd-ox, *1%*SnO_x@2AP-ox and *1%*SnO_x@2AP-H_2.

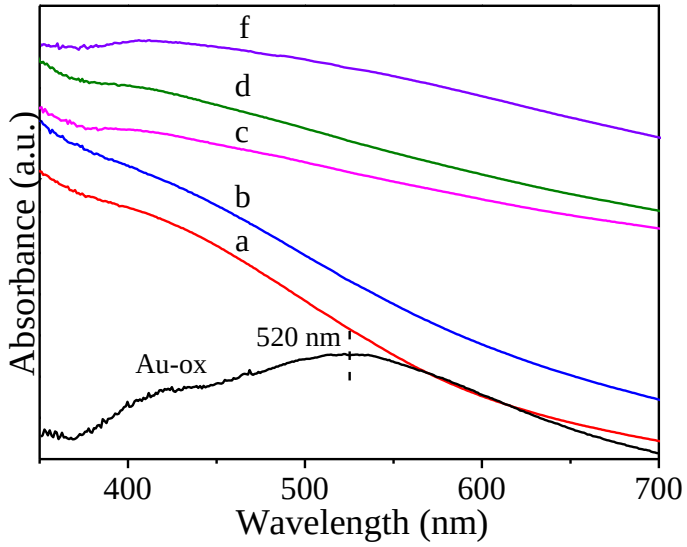

Figure 2. Solid UV-vis spectra of catalysts: (a) Pd-ox, (b) AP-ox, (c) 0.2%SnO_x@AP-ox, (d) 0.5%SnO_x@AP-ox, (e) 1.0%SnO_x@AP-ox, (f) 0.5%SnOx@AP-H_2.

Different amounts of SnO_x were introduced into the bimetallic AP-ox catalysts with constant Au (~0.25*wt.* %) and Pd (~0.5*wt.*%) contents. The actual metal content was determined by ICP-OES and the results are summarized in Table 1. The XRD

patterns of catalysts in the range of 19.5-70.5° 2θ reveal the weak diffraction peaks due to the presence of Pd, Au-Pd and PdO (Figure S1C). Catalysts with high metal loadings were prepared to clarify the peak positions of metals and oxides (Figure 1). Both 2Pd-ox and 2AP-ox catalysts contain a diffraction peak at 33.69^{o} 2θ corresponding to the PdO (110) (PDF#06-0515). No reduction of the catalysts was carried out and therefore the PdO is present.[8] After introducing the SnO_x on catalyst 1%SnO_x@2AP-ox, the intensity of the characteristic PdO phase peak at 2θ = 33.69^{o} was reduced. The peaks at 40.1^{o} and 46.6^{o} 2θ corresponding to (111) and (200) planes of cubic Pd (PDF#65-2867) shifted to lower 38.9^{o} and 45.3^{o} 2θ for catalyst 1%SnO_x@2AP-ox, respectively, which was attributed to the formation of Au-Pd(111) phase.[30] This result is in accordance with XRD pattern of catalyst 2AP-H_2 shown in Figure 1. After reduction, two diffraction peaks at 39.9^{o} and 41.0^{o} 2θ were observed for catalyst 1%SnO_x@2AP-H_2, similar to the diffraction peaks detected for the 1%SnO_x@2Pd-H_2. The peak at 39.9^{o} 2θ can be assigned to the cubic Pd (111) plane (40.1^{o}), while the peak at 41.0^{o} 2θ is due to PdSn (111) phase. These results revealed that the H_2 reduction treatment weakens the interactions between Au and Pd leading to the formation of Pd-Sn alloy. No obvious Sn or SnO_x species were detected on these catalysts, implying either a good dispersion or amorphous Sn species.[31] Concisely, Pd exists as PdO species on unpromoted catalysts 2Pd-ox and 2AP-ox, but partially as Au-Pd alloy species on SnO_x promoted 1%SnO_x@2AP-ox catalyst. This phase variation indicated that the introduction of SnO_x led to partial reduction of PdO and promoted the formation of the Au-Pd alloy, which is probably due to the electron

transfer from SnO_x to PdO,[32-33] due to the lower electronegativity and stronger oxophilicity of Sn than Pd.[34] As shown in Figure S1C, the same trend was observed for catalysts *y*SnO_x@AP-ox(H_2) with different SnO_x concentrations; low intensity of the Bragg peaks is due to the low metal loadings.

The UV-vis spectra of catalysts *y*SnO_x@AP-ox and *y*SnO_x@AP-H_2 are shown in Figure 2 and Figure S2, respectively. A broad peak at around 520 nm for monometallic catalyst Au-ox is attributed to the surface plasma resonance (SPR) of Au^0 NPs.[35] However, on bimetallic AP-ox and SnO_x promoted *y*SnO_x@AP-ox catalysts the characteristic peak of Au NPs is not observed, indicating the formation of Au-Pd alloy NPs on these catalysts (Figure 1) and also Au was no longer present as a pure metallic particle.[1] Even after H_2 reduction at 300 ^oC (*y*SnO_x@AP-H_2), no bands corresponding to the Au NPs were observed in the UV-vis spectra, revealing that Au still exists as alloy species (Au-Pd-Sn) (Figure S2). Further elevated reduction temperature to 400 ^oC and 500 ^oC did not lead to obvious Au phase formation (Figure S3), no SPR of Au NPs (clusters) were detected even after reduction at 500 ^oC for 2h. Based on the above results, we could conclude that H_2 reduction weakens the interaction between Au and Pd and no pure Au phase was present, implying that probably Au-Pd-Sn alloy is the dominant phase in the sample.

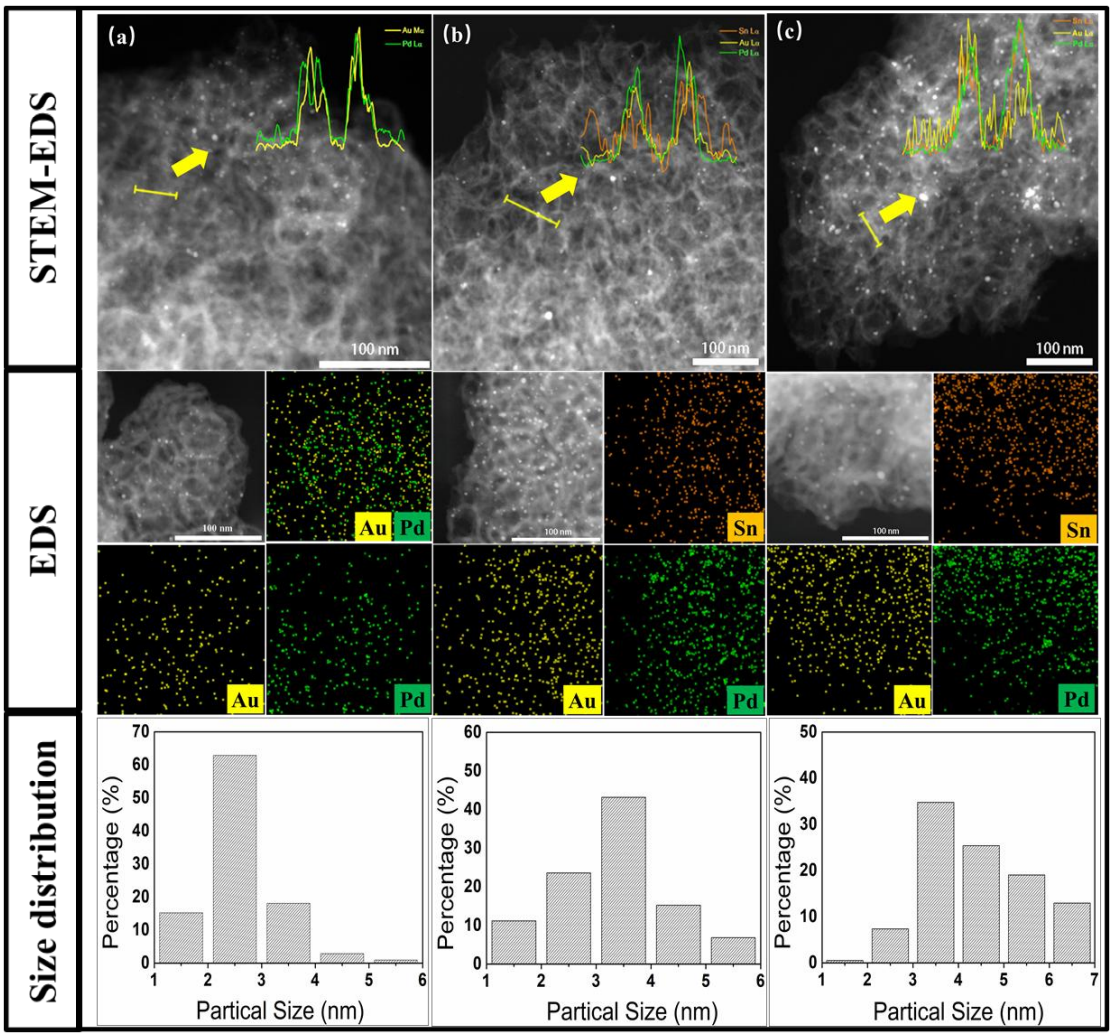

Figure 3. STEM-HAADF images of catalysts (*Insets:* energy dispersive line scan across NPs using the Au-M, Pd-L and Sn-L X-rays) and the corresponding EDS spectral maps of Au (yellow), Pd (green) and Sn (orange) and particle size distribution histograms of catalysts (a) AP-ox, (b) 0.5%SnO_x@AP-ox and (c) 0.5%SnO_x@AP-H_2.

Figure 3 shows representative STEM-HAADF images and EDS spectral maps, and the histograms of the particle size distribution of catalysts AP-ox, 0.5%SnO_x@AP-ox and 0.5%SnO_x@AP-H_2. The size effect of the NP catalyst and the distribution of metal elements play important roles in their catalytic performance.[23, 36] The representative STEM-HAADF images and the corresponding EDS spectral maps of

catalyst AP-ox indicated the presence of well-dispersed Au and Pd on the MCF support. Moreover, the energy dispersive line scan across NPs revealed the consistent dispersion of these two elements, indicating the formation of Au-Pd nano-alloys, which is in agreement with the UV-vis results. After introducing SnO_x, a slight increase of NPs size (2-6nm) was observed on catalyst 0.5%SnO_x@AP-ox comparing with that (2-4nm) on catalyst AP-ox, which was probably due to the dispersion of SnO_x on Au-Pd NPs. The energy dispersive line scan across the NPs indicated that the dispersion of Sn atoms was identical to that of Au-Pd.[37] After the reduction, the intensity of Sn signal was significantly enhanced on catalyst 0.5%SnO_x@AP-H_2 and this result is indicating the aggregation of Sn on Au-Pd NPs and formation of Au-Pd-Sn NPs with uniform composition. The introduction of SnO_x resulted in a slight increase of metal particle size for catalyst 0.5%SnO_x@AP-ox and a further increase of particle size on reduced catalyst 0.5%SnO_x@AP-H_2 (3-7 nm), which is probably due to the reduction process leading to enhanced interaction between Au-Pd NPs and Sn and aggregation into larger NPs.

To further study the chemical composition of alloy NPs before and after H_2 reduction, the high-resolution HAADF images and corresponding element analysis spectra of catalysts 0.5%SnO_x@AP-ox and 0.5%SnO_x@AP-H_2 were recorded by AC-TEM (Figure 4). Energy-dispersive line-scanning spectra (Figure 4b) show a much higher signal intensity of Au and Pd than that of Sn on catalyst 0.5%SnO_x@AP-ox. EDS elemental mapping (Figure 4d-f) further verified the homogenous dispersion of Au and Pd, confirming the formation of Au-Pd alloy NPs.

Correlating the line-scanning spectra shown in Figure 4b with EDS mapping of Sn element (Figure 4f), it can be concluded that SnO_x was successfully deposited on Au-Pd NPs of the un-reduced catalyst 0.5%SnO_x@AP-ox. The Sn element evenly distributed on the surface of catalyst 0.5%SnO_x@AP-ox (Figure 4b). By contrast, an obvious accumulation of Sn element on Au-Pd alloy NPs was observed through line scan (Figure 4b') and elemental mapping (Figure 4f') on the H_2-reduced catalyst 0.5%SnO_x@AP-H_2, and the nanoparticles were morphologically structured with an Au-Pd rich core and a Sn-rich shell. These results revealed the structure reconstruction of alloy NPs and presence of strong interaction between Au-Pd NPs and Sn after H_2 reduction. These observations are in line with the XRD and TEM results.

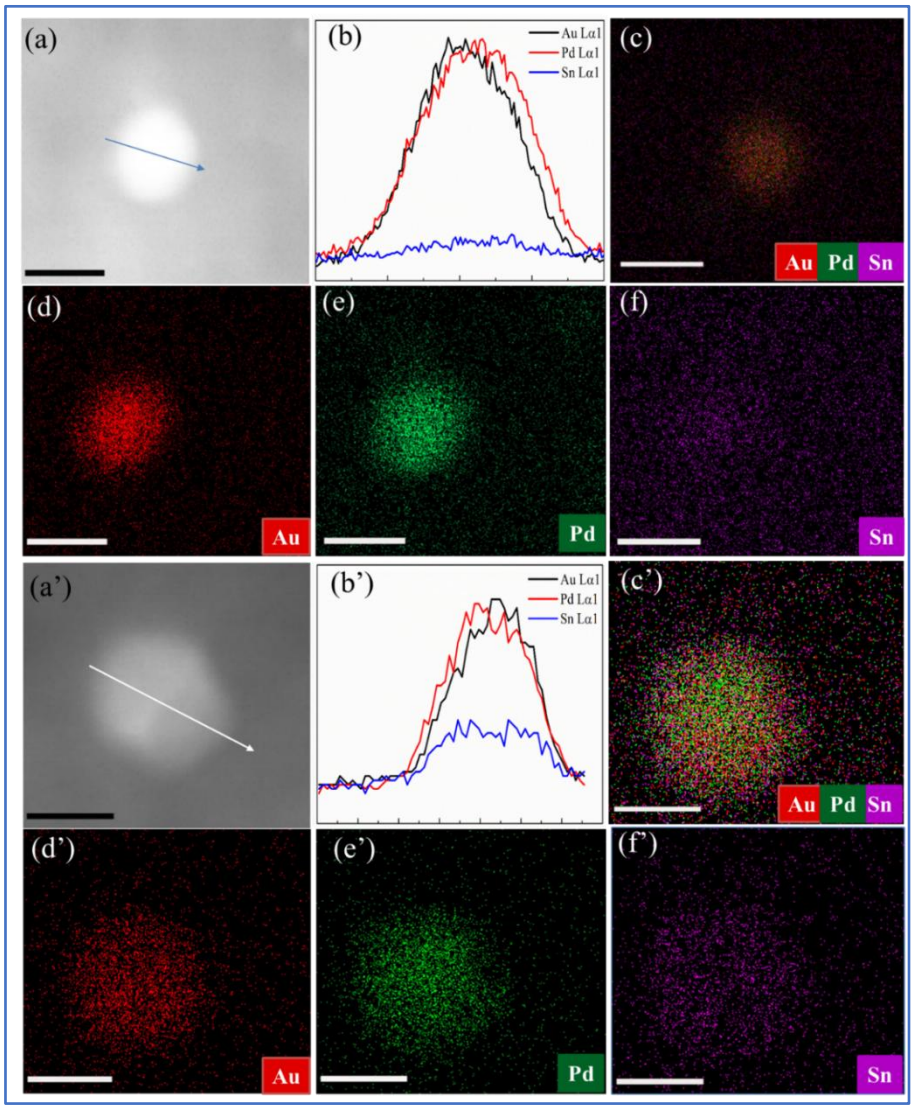

Figure 4. High resolution HAADF-STEM images with energy-dispersive line-scans of a single nanoparticle and elemental maps of Au, Pd, Sn and merged (Au-Pd-Sn) images of catalysts 0.5%SnO_x@AP-ox (a-f) and 0.5%SnO_x@AP-H_2 (a'-f'). Scale bar, M=5 nm.

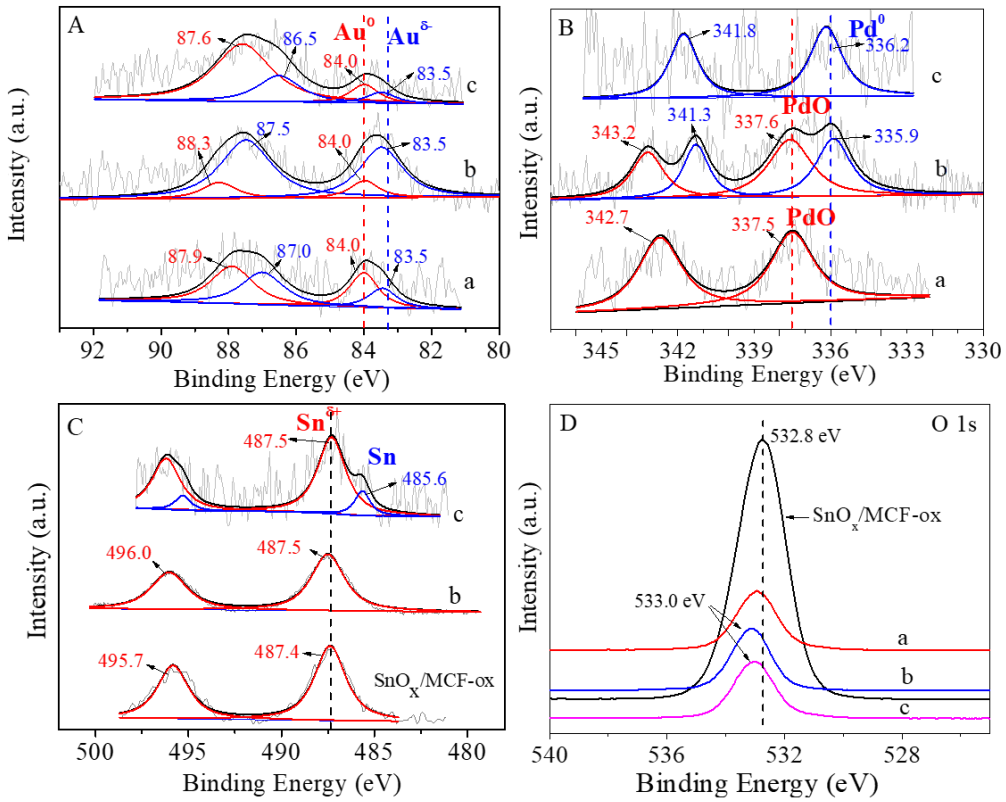

Figure 5. Au 4f XPS spectra (A), Pd 3d XPS spectra (B), Sn 3d XPS spectra (C) and O 1s XPS spectra (D) of catalysts: (a) AP-ox, (b) 0.5%SnO_x@AP-ox, (c) 0.5%SnO_x@AP-H_2 and a reference sample 1%SnO_x/MCF-ox.

The XPS spectra of Au 4f, Pd 3d, Sn 3d, and O 1s are shown in Figure 5A-5D and the detailed surface states of elements are summarized in Table 2. The XPS spectra of Au 4f indicated the presence of two types of Au species ($Au^{\delta-}$ and Au^0) on the catalysts.[38-39] The two characteristic peaks with binding energies (BE) of 84.0 eV (Au4$f_{7/2}$) and 87.9 eV (Au4$f_{5/2}$) were observed on the bimetallic catalyst AP-ox, corresponding to the typical Au^0 species.[40] While the other two peaks with BEs of 83.5 eV and 87.0 eV are attributed to the presence of negatively charged $Au^{\delta-}$ species.[41] The formation of $Au^{\delta-}$ species on bimetallic catalysts was due to the alloying effect of Au and Pd, the electrons can easily transfer from Pd to Au to form

negatively charged $Au^{\delta-}$.[42] These four peaks were also observed on catalyst 0.5%SnO_x@AP-ox, indicating the existence of Au^0 and $Au^{\delta-}$species,[40-41] however, the ratio of surface $Au^{\delta-}/Au^0$ changed drastically from 0.6 for catalyst AP-ox to 4.5 for catalyst 0.5%SnO_x@AP-ox. The low surface $Au^{\delta-}$ content for catalyst AP-ox was due to the presence of surface PdO species as shown by XRD; the Au cannot alloy with PdO.[11] Whereas the introduction of SnO_x promoted the reduction of PdO and formation of Au-Pd alloy NPs and increase the amount of surface $Au^{\delta-}$ species. On the reduced catalyst 0.5%SnO_x@AP-H_2, the $Au^{\delta-}/Au^0$ ratio decreased to 1.7 due to the partial reduction of SnO_x to Sn and its alloying with Au-Pd to form Au-Pd-Sn alloy NPs. The latest weakened the interaction between Au and Pd and resulted in a decrease of electron density of the Au surface.

For 3d Pd XPS spectra contain the $3d_{5/2}$ with BE of 335.5±0.3eV corresponds to Pd^0 species[43-45] and the $3d_{5/2}$ with BE of 337.5±0.3eV corresponds to Pd^{2+}(PdO) species.[43-44] The Pd XPS spectrum (Figure 5B) of the AP-ox bimetallic catalyst contains a peak with BE of 337.5 eV corresponding to PdO species.[46] On SnO_x promoted catalyst (0.5%SnO_x@AP-ox), two Pd $3d_{5/2}$ characterization peaks with BE of 335.9 eV and 337.6 eV corresponding to Pd^0 and PdO, respectively, are present.[46] These results are in accordance with the XRD data, revealing that the introduction of SnO_x leads to a partial reduction of PdO to Pd^0 species, which is due to the higher oxophilicity of Sn with lower electronegativity than the Pd (Sn=1.96, Pd=2.20).[34] On the H_2 reduced catalyst (0.5%SnO_x@AP-H_2), the Pd^0 species with BE of 336.2 eV,[47]

with a slight positive shift (0.3 eV) probably due to the strong interaction between Sn and Pd is observed.

The Sn 3d XPS spectrum of the reference sample (SnO_x/MCF-ox) contains peaks at 487.3 eV($3d_{5/2}$) and 495.7 eV($3d_{3/2}$) corresponding to the presence of SnO_2 species (Figure 5C). The spectrum of catalyst 0.5%SnO_x@AP-ox contains a peak slightly shifted to higher binding energy (487.5 eV) confirming the presence of SnO_2. This positive BE shift is generally attributed to the strong interaction between Au-Pd NPs and SnO_2 in which an electron transfer from SnO_2 to Au-Pd occurred,[48] resulting in partial reduction of PdO to Pd^0 and formation of more surface $Au^{\delta-}$ species as shown in Figure 5A, B. However, on the reduced catalyst 0.5%SnO_x@AP-H_2, typical Sn^0 species with BE of 485.5 eV were detected in addition to the SnO_2, indicating that SnO_2 was partially reduced under H_2 at 300 ^oC. In summary, electrons transfer from SnO_2 species to Au and Pd on catalyst 0.5%SnO_x@AP-ox, leading to the formation of Au-Pd alloy NPs was observed. As low-coordinated Pd^0-enriched clusters are generally considered as active sites for benzyl alcohol oxidation, [13,49] introducing SnO_x to AP-ox catalyst increased the active sites of catalyst 0.5%SnO_x@AP-ox, which could cause an enhancement of catalytic activity for benzyl alcohol oxidation. After the reduction, the PdO was completely reduced to Pd^0, and SnO_x was partially reduced to Sn. The strong interaction between Pd and Sn species leaded to the formation of Au-Pd-Sn alloy as confirmed by correlating the UV-Vis and XRD results. The O 1s XPS spectrum of sample 1%SnO_x/MCF-ox contains a lower energy band (532.8 eV) implying that there are more electron-rich oxygen atoms near the

surface of the metal oxide (Figure 5D). While for the 0.5%SnO_x@AP-ox, the binding energy shifted to higher value (533.0 eV), indicating the weakening of surface metal oxygen (M-O) interactions.

Table 2. Surface Composition of Catalysts.

Samples	ICP	XPS	XPS		
	Au: Pd: Sn	Au: Pd: Sn	$Au^{\delta-}$: Au^0	Pd^0: Pd^{2+}	Sn^0: $Sn^{\delta+}$
AP-ox	1: 3.6: 0	1: 2.3: 0	0.6: 1	0: 1:	---
0.5%SnO_x@AP-ox	1: 3.6: 2.8	1: 6.0: 23.8	4.5: 1	1: 1.2	0: 1
0.5%SnO_x@AP-H_2	1: 3.6: 2.8	1: 4.1: 6.3	1.7: 1	1: 0	0.2: 1
0.5%SnO_x@AP-ox[a]	1: 3.7: 2.6	0: 1: 8.6	undetectable	1: 0.25	0: 1

[a] Catalyst 0.5%SnO_x@AP-ox was analyzed after a control reaction in N_2 atmosphere.

The bulk atomic ratio of Au/Pd/Sn based on ICP and surface chemical composition based on XPS of different catalysts are summarized in Table 2. The atomic ratio of Au/Pd/Sn in the bulk of the 0.5%SnO_x@AP-ox catalyst is 1: 3.6: 2.8, while the surface composition was found to be 1: 6.0: 23.8 on the same catalyst. This result confirmed that most of Sn is distributed on the catalysts surface, which is consistent with EDX analysis (see line-scans and mapping in Figure 4). After the reduction, the Au/Pd/Sn ratio on the surface was dramatically changed to 1: 4.1: 6.3, indicating that Sn partially entered in the bulk of NPs. This observation is consistent with the STEM-HADDF results showing that the reduction led to the transformation of surface Sn to the bulk, which may result in the formation of Au-Pd-Sn alloy NPs,

and/or a reduced SnO_x shell with different spreading on the Au-Pd particles. Furthermore, the strong interaction between Pd and Sn weakened the interaction between Au and Pd, thus leading to the electron redistribution between Au-Pd-Sn atoms.

H_2-TPR profiles of the catalysts are depicted in Figure 6A. The spectrum of monometallic catalyst Pd-ox contains a peak at 106 °C which is commonly attributed to the reduction of surface PdO species and a peak at 267°C ascribed to the reduction of bulk PdO. While in the spectrum of bimetallic catalyst AP-ox, the bulk reduction peak at 267°C disappeared, indicating alloying of Au and Pd that prevented the formation of bulk PdO phase.[8-10] A negative reduction peak at 59 °C was observed for catalysts 0.2%SnO_x@AP-ox, 0.5%SnO_x@AP-ox and 1.0%SnO_x@AP-ox, which could be attributed to the decomposition of β-PdH_x. Since PdO species are easily reduced in a hydrogen atmosphere to metallic Pd, which further interacts with hydrogen to form β-PdH_x species.[50-51] The presence of this peak indicated that PdO species on SnO_x promoted catalysts are easily reduced to active Pd^0 species or the Pd^0 species are present. A reduction peak around 525°C is observed for sample SnO_x@MCF-ox, which is due to the reduction of surface SnO_x species, however, this peak shifts to 370°C for catalysts 0.5%SnO_x@AP-ox and 1.0%SnO_x@AP-ox, revealing that the interaction between SnO_x and Au-Pd NPs promotes the reduction of surface SnO_x species. Combined the H_2-TPR with XPS results, one can conclude that the strong interaction between SnO_x and Au-Pd NPs helps the reduction of surface

SnO_x and PdO species, which may act as oxygen transfer intermediate during the oxidation reaction.

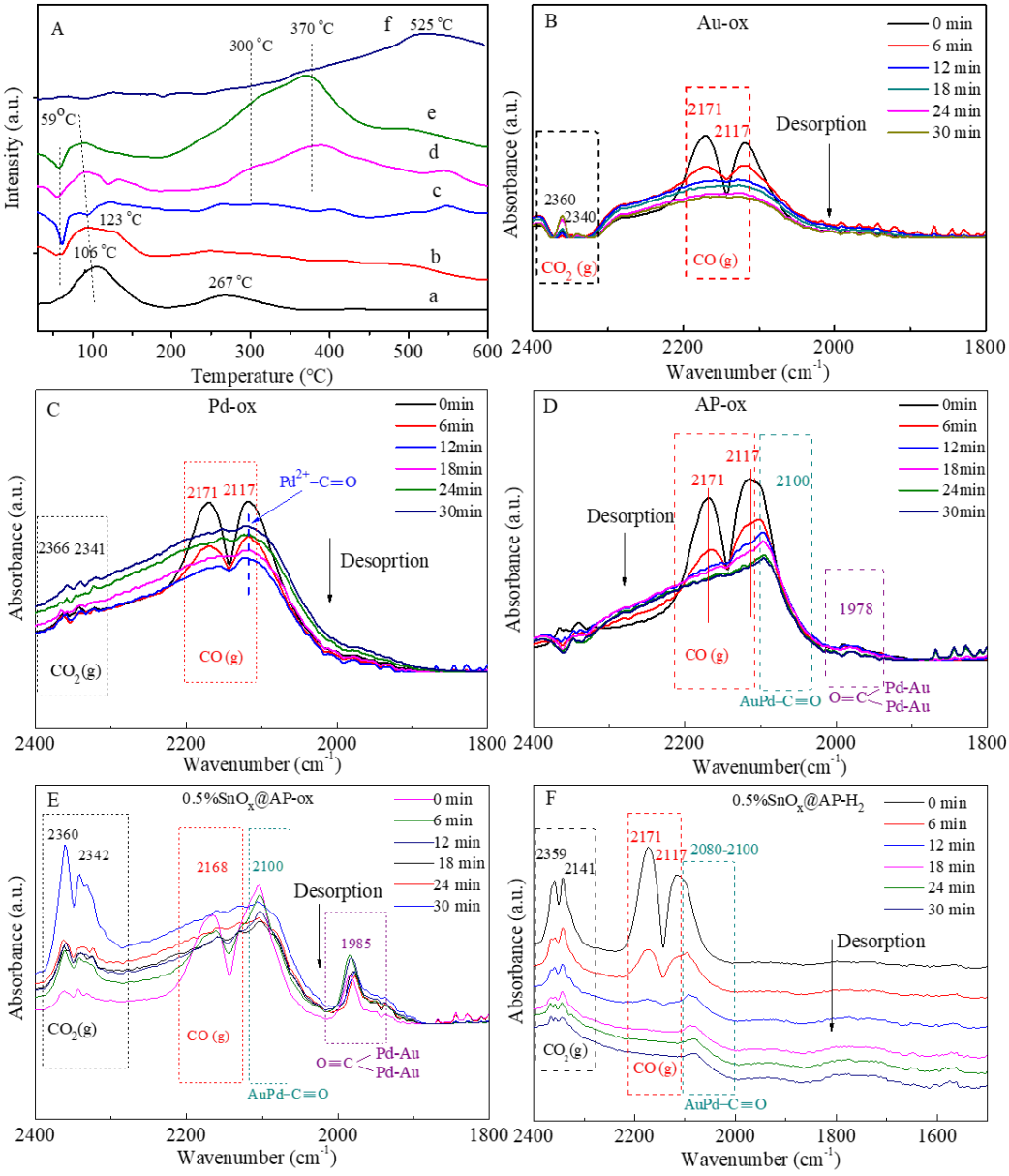

Figure 6. H_2-TPR spectra (A) of catalysts (a) Pd-ox, (b) AP-ox, (c) 0.2%SnO_x@AP-ox, (d) 0.5%SnO_x@AP-ox, (e) 1.0%SnO_x@AP-ox and (f) SnO_x@MCF-ox. Time-resolved CO-desorption DRIFTS spectra of catalysts (B) Au

-ox, (C) Pd -ox, (D) AP-ox, (E) 0.5%SnO_x@AP-ox and (F) 0.5%SnO_x@AP-H_2 at 25ºC.

The time-resolved CO adsorption DRIFTS spectra were conducted for all catalysts and presented in Figure 6B-F and Figure S4-5 (full spectral range). The bands at 2171 cm^{-1} and ~2117 cm^{-1} are observed in the spectra for all samples and their intensity decreased with the CO desorption, which are ascribed to the physically adsorbed gaseous CO.[52] The typical CO adsorption on Au at 2100 ~ 2000 cm^{-1} was not obvious[53] on catalyst Au -ox (Figure 6B), which is probably due to the strong interaction between Au NPs and silica support.[8] For catalyst Pd-ox (Figure 6C), the carbonyls on Pd^{2+} at 2117 cm^{-1} overlapping with adsorption bands of gaseous CO are confirmed,[54] and this band does not disappear during CO desorption. A new band at ~2100cm^{-1} was observed on the bimetallic catalyst AP-ox (Figure 6D). The intensity of the latest band was enhanced for catalyst 0.5%SnO_x@AP-ox (Figure 6E), associated with the linearly adsorbed CO on $Pd^{\delta+}$ located in the corner or edge sites of Pd nanoparticles [55-56]. A weak adsorption band centered at 1985 cm^{-1} is present in the spectrum of catalysts AP-ox (Figure 6D) due to bridged CO adsorption on contiguous Pd^0 sites or Pd^0-enriched clusters (ν_{CO}: 1900 – 2000 cm^{-1})[57] that was further enhanced for catalyst 0.5%SnO_x@AP-ox (Figure 6E), indicating the formation of Pd^0-enriched clusters after introducing SnO_x. Whereas, the enhanced intensity of the band at ~2100cm^{-1} reflecting the increase of linearly adsorbed CO on Pd^0 sites. These results reveal the increase of both Pd^0-enriched clusters and single Pd^0 sites on catalyst 0.5%SnO_x@AP-ox, which is consistent with XRD and XPS results. After H_2

reduction (Figure 6F), the band corresponding to the bridged adsorption of CO on Pd^0 at 1985 cm^{-1} disappeared, indicating the reconstruction of Pd^0-enriched clusters to Au-Pd-Sn or Pd-Sn alloy NPs. The CO_2 vibration peaks (~2360 and ~2340 cm^{-1})[52] were detected on SnO_x promoted catalysts 0.5%SnO_x@AP-ox and 0.5%SnO_x@AP-H_2, revealing that CO was readily oxidized to CO_2 on these catalysts at room temperature (25°C). Especially on unreduced catalyst 0.5%SnO_x@AP-ox, the intensity of CO_2 adsorption bands increased as the desorption proceeds (Figure 6E, black frame), indicating that the adsorbed gaseous CO was oxidized to CO_2. These results indicated that SnO_x could serve as an oxygen transfer medium which would enhance the oxygen transfer during partial oxidation of benzyl alcohol over Au-Pd NPs catalyst.

3.2 Catalytic Evaluation. The activity for benzyl alcohol oxidation and benzaldehyde selectivity of different catalysts are presented in Figure 7A; detailed oxidation results are summarized in Table S1. The external and internal diffusion limitations have been neglected based on the results from our recent study.[58] Therefore, the TOFs is used to represent the intrinsic activity of catalysts in the current study. As is shown (Figure 7A and Table S1), the catalytic activity on unreduced monometallic catalysts (Au, Pd, Sn) and bimetallic catalysts (Au-Pd, Au-Sn, Pd-Sn) are low. But a significant enhancement of catalytic activity was achieved on SnO_x promoted catalyst 0.5%SnO_x@AP-ox, indicating a synergy among different Au, SnO_x and Pd species. Catalyst AP-ox exhibited a low catalytic activity (TOF=4365h^{-1}) for benzyl alcohol oxidation because inert PdO species exist as the

dominant surface species (see XPS spectra, Figure 4B). After introducing 0.5wt.% SnO_x, a higher catalytic activity (TOF=13662 h^{-1}) was achieved on catalyst 0.5%SnO_x@AP-ox, due to the presence of active Pd^0 species on the catalyst surface. Thus, the introduction of SnO_x promoted the partial reduction of PdO to Pd^0 and formation of more Pd^0-enriched clusters on catalyst 0.5%SnO_x@AP-ox, leading to catalytic activity enhancement. However, the catalytic activity decreases on the H_2 reduced catalyst 0.5%SnO_x@AP-H_2, where most of PdO species are believed to be reduced to Pd^0. The low catalytic activity of catalyst 0.5%SnO_x@AP-H_2 is due to the formation of Au-Pd-Sn alloy NPs with uniform composition, which results in the decrease of active Pd^0-enriched clusters as shown by CO adsorption FT-IR.[13] It is also noted that no obvious enhancement of catalytic activity was observed on SnO_x promoted Pd NP catalysts no matter whether were or not treated under H_2 (catalysts 0.5%SnO_x@Pd -ox and 0.5%SnO_x@Pd-H_2, TOF=7500-7800 h^{-1}), Table S1. These results indicate that the effect of Au on the catalyst performance should not be ignored. The role of Au on the Au-Pd alloy NP catalyst was usually considered as a structural and electronic promoter, which fostered the formation of active Pd^0-enriched sites. It is worth noting that a significant enhancement of benzaldehyde selectivity (from 60.1% on catalyst AP-ox to 73.2% on catalyst 0.5%SnO_x@AP-ox) was achieved after introducing the SnO_x promoter, and especially the benzaldehyde yield increased from 15.7% (AP-ox) to 59.8% (0.5%SnO_x@AP-ox) after 2h reaction. The benzaldehyde selectivity increased with the increase of SnO_x content, which should be related to the surface properties of the catalyst. Similar results were also

reported by Hutchings and coworkers for H_2O_2 synthesis.[13] SnO_x promoted Pd/TiO_2 catalyst exhibited high H_2O_2 selectivity attributable to the surface modification of SnO_x to Pd sites.

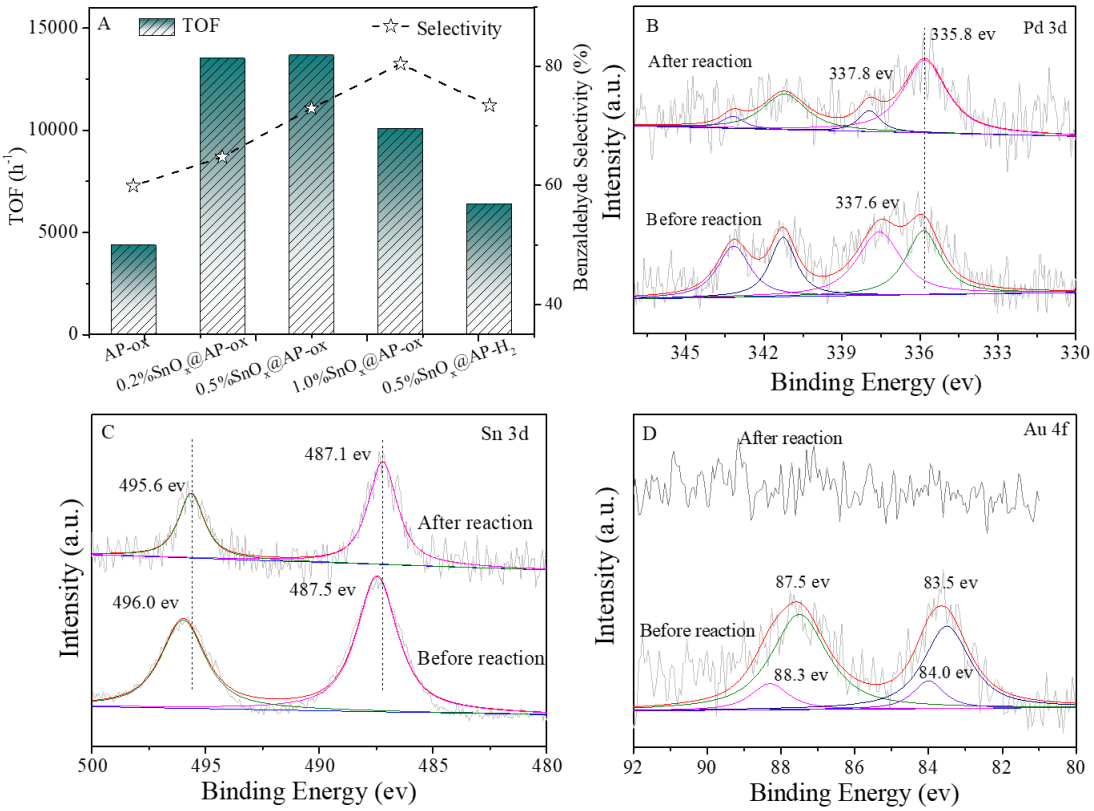

Figure 7. (A) Performance (TOF) of catalysts, XPS spectra of Pd 3d (B), Sn 3d (C), and Au 4f (D) before and after control reaction (reaction conditions: 50.0 mg catalyst, 10.8 g benzyl alcohol, nitrogen pressure of 0.8 MPa, reaction temperature of 110℃, reaction time of 2 h, stirring rate of 800 r/min).

In order to study the catalytic mechanism of benzyl alcohol oxidation on SnO_x promoted Au-Pd catalyst, the control reaction was carried out on catalyst $0.5\%SnO_x$@AP-ox under the same reaction conditions except for using N_2 atmosphere. A benzyl alcohol conversion of 5.8% with benzaldehyde selectivity of

85.3% were obtained after 2h reaction. The surface properties of the used catalyst were characterized by XPS, Figure 7B-D. A significant increase of Pd^0/Pd^{2+} ratio from 1:1.2 to 1:0.25 was observed after the reaction under N_2 atmosphere, indicating that PdO participates in the oxygen transfer during the oxidation reaction. The BE of Sn 3d shifted from 487.5eV to 487.1eV revealing the partial reduction of SnO_x to lower valance state $SnO_{x-\delta}$ (Figure 7C). However, no surface Au species are detected after the reaction. ICP results revealed no obvious leaching of Au during the control reaction (Table 2). These results indicated that both PdO and SnO_2 were reduced in the control reaction, namely participating in the oxygen transfer during the oxidation, which is in good accordance with time resolved CO-DRIFTS data. The surface Pd/Sn ratio decreased from 0.25 to 0.12 after the reaction, indicating the surface accumulation of Sn on Au-Pd-Sn NPs, while Au transferred to the inner bulk or covered by Sn-Pd.

Correlating the characterization results with the activity of the catalyst ($0.5\%SnO_x$@AP-ox), we could conclude that the introduction of SnO_x promotes the partial reduction of surface PdO to active Pd^0 species. Both PdO and SnO_x participated in the oxygen transfer reaction, leading to a high catalytic activity. After H_2 reduction, the PdO was completely reduced to Pd^0, while SnO_x was partially reduced and migrated to the bulk of Au-Pd NPs to form Au-Pd-Sn alloy NPs. A low catalytic activity was observed on catalyst $0.5\%SnO_x$@AP-H_2, which is due to the formation of surface Au-Pd-Sn alloy.

3.3 DFT Calculation. The DFT calculations were applied to further explain the reconstruction of active sites on SnO_x promoted Au-Pd catalysts and the results are shown in Table 3. It was found that the bond energy of Sn-O is 141.1 kcal/mol, which is significantly higher than that of the Pd-O bond (86.8 kcal/mol), therefore, part of PdO species would be reduced by Sn and more Pd^0 sites were generated after introducing Sn (XPS results). Simultaneously, the formation energy of different alloys was calculated to verify the reconstruction of active sites after H_2 reduction. The results indicated that the absolute value of Pd_3Au formation energy (-0.43 eV) is quite smaller than that of Pd_3Sn (-1.84 eV), which explained the easy formation of Pd-Sn/Au-Pd-Sn alloy after H_2 reduction and justified the experimental results.

Table 3. The bond energies of different M-O bonds and formation energies of different alloys.

M-O	Bond energy (kcal/mol)	Alloys	E_f (eV)
Sn-O	-141.2	Pd_3Au	-0.43
OSn-O	-76.3	Pd_3Sn	-1.84
Pd-O	-86.8		

$E_f = [E(Pd_iM_j) - iE(Pd) - jE(M)]/(i + j)$, E ($Pd_iM_j$) represents the total energy of the Pd_iM_j alloy unit cell, E (Pd) and E (M) represent the energy of each atom in Pd and M simplex, respectively, i and j represent the number of Pd and M atoms in the alloy unit cell, respectively.

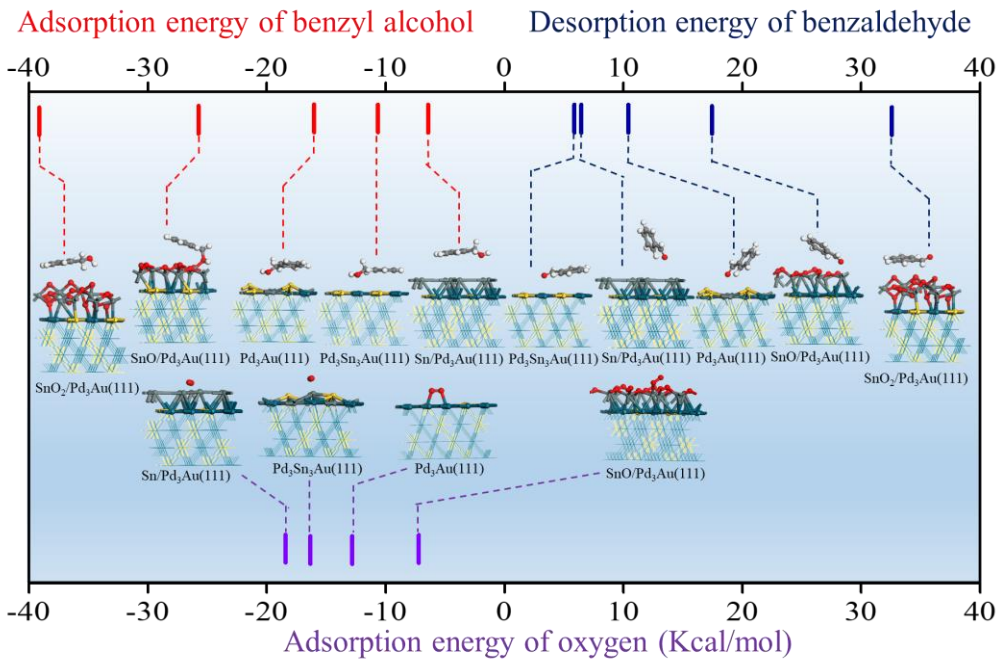

Figure 8. Adsorption/desorption energies and configurations of benzyl alcohol, O_2 and benzaldehyde on $Pd_3Au(111)$, $SnO_x/Pd_3Au(111)$, $Sn_3Pd_3Au(111)$ and $Sn/Pd_3Au(111)$ surfaces (blue, yellow, gray in the catalyst, gray in the benzene ring, red, and white balls denote Pd, Au, Sn, C, O, and H atoms, respectively). Note: The adsorption energy and desorption energy are calculated by the same equation but with opposite values. The term of adsorption energy was applied for reactants (benzyl alcohol and oxygen), while the term of desorption energy was applied for product for distinction.

The catalytic activity and useful product selectivity of benzyl alcohol partial oxidation were closely related to the adsorption properties and surface O species.[59-60] Thus, the adsorption/desorption energies and configurations of benzyl alcohol, O_2 and benzaldehyde on $Pd_3Au(111)$, $Sn_3Pd_3Au(111)$, $Sn/Pd_3Au(111)$, $SnO/Pd_3Au(111)$, and $SnO_2/Pd_3Au(111)$, whereas the detailed energy barrier for the O_2 decomposition into 2

O, the adsorption energy of benzyl alcohol and oxygen, and the desorption energy of the products are presented in Figure 8 and listed in Table S2. Compared with the bimetallic $Pd_3Au(111)$ surface, the Sn containing surfaces (Sn/Pd_3Au (111) and $SnO/Pd_3Au(111)$) are conducive for the adsorption and activation of oxygen molecules, since the decomposition energy barrier of the O_2 decomposition is significantly reduced from 42.5 kcal/mol on the $Pd_3Au(111)$ surface to 19.2 kcal/mol on the $Sn/Pd_3Au(111)$ surface and to 33.5 kcal/mol on the $SnO/Pd_3Au(111)$ surface. The adsorption energies of benzyl alcohol on the $SnO/Pd_3Au(111)$ and $SnO_2/Pd_3Au(111)$ surfaces are 32.0 kcal/mol and 39.2 kcal/mol, respectively, much higher than those of other surfaces, indicating that benzyl alcohol could be easily adsorbed on the $SnO/Pd_3Au(111)$ and $SnO_2/Pd_3Au(111)$ interfaces. On the other hand, the adsorption energy of benzaldehyde on the reduced surfaces ($SnO/Pd_3Au(111)$ and $Sn/Pd_3Au(111)$) is lower than that on the surface of $SnO_2/Pd_3Au(111)$, which indicates benzaldehyde easily desorbed from the $SnO/Pd_3Au(111)$ or $Sn/Pd_3Au(111)$ interface. The characterization results revealed that SnO_2 participates in the oxygen transfer reaction and is partially reduced during the reaction (Figure 7C). Benzyl alcohol was easily adsorbed on the SnO_2/Pd_3Au (111) surface and oxidized by SnO_2, and at the same time, the SnO_2/Pd_3Au (111) interface was reduced to $SnO/Pd_3Au(111)$ or $Sn/Pd_3Au(111)$ which are beneficial for the benzaldehyde desorption. The reduced interfaces SnO/Pd_3Au (111) and $Sn/Pd_3Au(111)$ continue to adsorb oxygen and participate in the next reaction cycle (Figure 9A). However, when the catalyst was completely reduced (Pd_3Sn_3Au alloy formation), the adsorption energies of benzyl

alcohol decreased (from 16.2 kcal/mol on $AuPd_3$ alloy to 10.5 kcal/mol on Pd_3Sn_3Au alloy), the adsorption distance increased (2.502Å→2.698Å), thus, leading to a low catalytic activity on H_2-reduced catalyst 0.5%SnO_x@AP-H_2.

Based on the above results, a reaction mechanism was proposed (Figure 9B). The enhanced catalytic activity on SnO_x promoted AP catalyst was due to the presence of high oxophilic Sn, which promoted the partial reduction of PdO to active Pd^0. Both PdO and SnO_x participated in the partial oxidation reaction and enhanced the O transfer, thus leading to a high catalytic activity. The redox switching of SnO_x with $SnO_{x-\delta}$ changed the catalyst surface affinity to benzyl alcohol and benzaldehyde. Benzyl alcohol was easily adsorbed on $SnO_2/Pd_3Au(111)$ surface, and SnO_2 participated in the oxygen transfer via reduction to $SnO/Pd_3Au(111)$ or $Sn/Pd_3Au(111)$, which is crucial for the benzaldehyde desorption, leading to a high benzaldehyde selectivity. The SnO/Pd_3Au or Sn/Pd_3Au reduced surfaces readily adsorb and react with oxygen to form SnO_2/Pd_3Au and participate in the next reaction cycle.

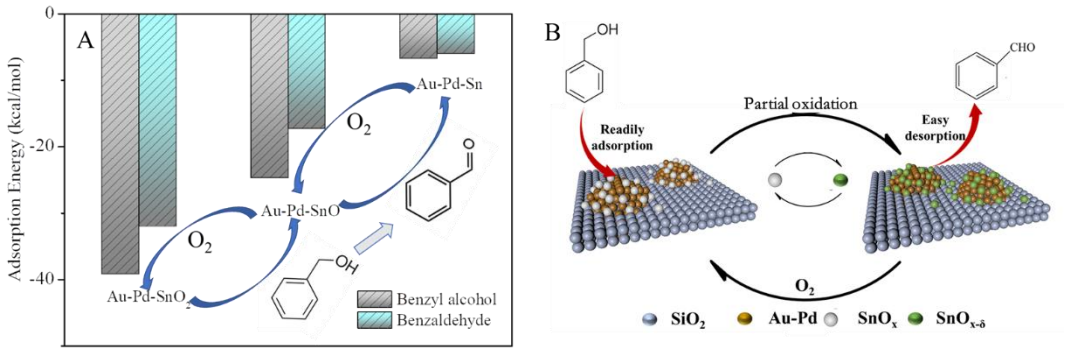

Figure 9. (A) Adsorption energy of benzyl alcohol and benzaldehyde on $SnO_2/Pd_3Au(111)$, $SnO/Pd_3Au(111)$ and $Sn/Pd_3Au(111)$ surfaces, and (B) Schematic

illustration of benzyl alcohol and benzaldehyde adsorption/desorption on SnO_x/Au-Pd and $SnO_{x-\delta}$/Au-Pd surface.

4. CONCLUSIONS

In this study, SnO_x was introduced into the Au-Pd bimetal catalyst as a promoter. Based on the comprehensive experimental and theoretical results we found out that the introduction of SnO_x promotes the partial reduction of PdO to active Pd^0-enriched clusters on unreduced catalyst, which is due to the high oxophilicity of Sn. The presence of more active Pd^0-enriched clusters, together with the enhancement of O transfer by PdO and SnO_x, results in the highest catalytic activity (13662 h^{-1}) for benzyl alcohol oxidation on catalyst 0.5%SnO_x@AP-ox, while the benzaldehyde selectivity increased with SnO_x ratio. The enhanced benzaldehyde selectivity on SnO_x promoted catalysts *y*SnO_x@AP-ox was due to the in-situ regulation of reactants and products affinity on the catalyst surface through redox switching of SnO_x with $SnO_{x-\delta}$ during oxidation reaction. After H_2 reduction, the SnO_x was partially reduced and Au-Pd-Sn alloy was formed leading to a reduced activity of the catalyst. The theoretical results revealed that the formation of Pd-Sn/Au-Pd-Sn alloy weakens the adsorption of benzyl alcohol on catalysts SnO_x@AP-H_2. In summary, the SnO_x promoted autogenous reduction of PdO to active Pd^0 species together with the enhancement of O transfer by PdO and SnO_x leading to high catalytic activity, while the SnO_x redox switching during the oxidation reaction modulated the adsorption properties of reactants and products which enhanced the benzaldehyde selectivity.

■ ASSOCIATED CONTENT

Supporting Information: N_2 adsorption/desorption isotherms; XRD spectra; Solid UV-vis spectra of reduced catalysts; DRIFT spectra using CO probe molecule adsorbed on different catalysts, the time-resolved DRIFTS spectra collected on different catalysts at 25 ^{o}C under 1% CO in He (in the full range); Catalyst benzyl alcohol oxidation results; Adsorption of benzyl alcohol, desorption of benzaldehyde, reaction energy barrier of O_2 and adsorption energy of oxygen on the catalyst surface.

■ AUTHOR INFORMATION

Corresponding Authors

Peng Bai- *State Key Laboratory of Heavy Oil Processing, Key Laboratory of Catalysis, College of Chemical Engineering, China University of Petroleum (East China), Qingdao 266580, China;*

Email: *baipeng@upc.edu.cn*

Lianming Zhao- *School of Materials Science and Engineering, Institute of Advanced Materials, China University of Petroleum (East China), Qingdao, 266580, China;*

Email: *lmzhao@upc.edu.cn*

Authors

Pingping Wu- *State Key Laboratory of Heavy Oil Processing, Key Laboratory of Catalysis, College of Chemical Engineering, China University of Petroleum (East China), Qingdao 266580, China;*

Zhengke He- *State Key Laboratory of Heavy Oil Processing, Key Laboratory of Catalysis, College of Chemical Engineering, China University of Petroleum (East China), Qingdao 266580, China;*

Yonghui Liu- *School of Materials Science and Engineering, Institute of Advanced Materials, China University of Petroleum (East China), Qingdao, 266580, China;*

Lei Song- *State Key Laboratory of Heavy Oil Processing, Key Laboratory of Catalysis, College of Chemical Engineering, China University of Petroleum (East China), Qingdao 266580, China;*

Edgar Muhumuza- *State Key Laboratory of Heavy Oil Processing, Key Laboratory of Catalysis, College of Chemical Engineering, China University of Petroleum (East China), Qingdao 266580, China;*

Svetlana Mintova- *Normandie University, ENSICAEN, UNICAEN, CNRS, Laboratoire Catalyse et Spectrochimie, 14000 Caen, France*

Zifeng Yan- *State Key Laboratory of Heavy Oil Processing, Key Laboratory of Catalysis, College of Chemical Engineering, China University of Petroleum (East China), Qingdao 266580, China;*

Notes

The authors declare no competing financial interest.

■ ACKNOWLEDGEMENTS

This work was financially supported by the Natural Science Foundation of China (51601223, 21908246, 21991090), the Fundamental Research Funds for the Central Universities (17CX05018, 17CX02056), Shandong Provincial Natural Science Foundation (ZR201702160196), State Key Laboratory of Heavy Oil Processing（SKLZZ-2017008) and the Sino-French International Laboratory (LIA) “Zeolites”.

REFERENCES

(1). He, Q.; Miedziak, P. J.; Kesavan, L.; Dimitratos, N.; Sankar, M.; Lopez-Sanchez, J. A.; Forde, M. M.; Edwards, J. K.; Knight, D. W.; Taylor, S. H. Switching-off Toluene Formation in the Solvent-free Oxidation of Benzyl Alcohol using Supported Trimetallic Au-Pd-Pt Nanoparticles. *Faraday Discuss.* **2013,** *162* (8), 365-378.

(2). Al-Saeedi, S.; Abdel-Rahman, L.; Abu-Dief, A.; Abdel-Fatah, S.; Alotaibi, T.; Alsalme, A.; Nafady, A. Catalytic Oxidation of Benzyl Alcohol Using Nanosized Cu/Ni Schiff-Base Complexes and Their Metal Oxide Nanoparticles. *Catalysts* **2018,** *8* (10), 452.

(3). Campisi, S.; Ferri, M.; Chan-Thaw, C. E.; Sanchez Trujillo, F. J.; Motta, D.; Tabanelli, T.; Dimitratos, N.; Villa, A. Metal-Support Cooperative Effects in Au/VPO for the Aerobic Oxidation of Benzyl Alcohol to Benzyl Benzoate. *Nanomaterials* **2019,** *9* (2), 299.

(4). Xiao, C.; Zhang, L.; Hao, H.; Wang, W. High Selective Oxidation of Benzyl Alcohol to Benzylaldehyde and Benzoic Acid with Surface Oxygen Vacancies on $W_{18}O_{49}$/Holey Ultrathin g-C_3N_4 Nanosheets. *ACS Sustainable Chem. Eng.* **2019,** *7* (7),

7268-7276.

(5). Ding, J.; Xu, W.; Wan, H.; Yuan, D.; Chen, C.; Wang, L.; Guan, G.; Dai, W.-L. Nitrogen Vacancy Engineered Graphitic C_3N_4-based Polymers for Photocatalytic Oxidation of Aromatic Alcohols to Aldehydes. *Appl. Catal. B-Environ.* **2018,** *221*, 626-634.

(6). Olmos, C. M.; Chinchilla, L. E.; Cappella, A. M.; Villa, A.; Delgado, J. J.; Hungría, A. B.; Blanco, G.; Calvino, J. J.; Prati, L.; Chen, X. Selective Oxidation of Veratryl Alcohol over Au-Pd/$Ce_{0.62}Zr_{0.38}O_2$ Catalysts Synthesized by Sol-Immobilization: Effect of Au: Pd Molar Ratio. *Nanomaterials* **2018,** *8* (9), 669.

(7). Xin, J.-y.; Fan, H.C.; Ji, S.F.; Wang, Y.; Xia, C.G. Methanobactin-mediated Synthesis of Bimetallic Au-Pd/Al_2O_3 Toward an Efficient Catalyst for Glucose Oxidation. *Iet Nanobiotechnol.* **2017,** *11* (5), 512-516.

(8). Wu, P.; Cao, Y.; Zhao, L.; Wang, Y.; He, Z.; Xing, W.; Bai, P.; Mintova, S.; Yan, Z. Formation of PdO on Au–Pd Bimetallic Catalysts and the Effect on Benzyl Alcohol Oxidation. *J. Catal.* **2019,** *375*, 32-43.

(9). Xu, J. W., T.; Li, P.; He, C.; Yu, J.; Yuan, W.; Han, Y.F. . Biphasic Pd−Au Alloy Catalyst for Low-Temperature CO Oxidation. *J. Am. Chem. Soc.* **2010,** *132*, 10398-10406.

(10). Li, Z. G., F.; Furlong, O.; Tysoe, W. T. Adsorption of Carbon Monoxide Au/Pd (100) Alloys in Ultrahigh Vacuum: Identification of Adsorption Sites. *Surf. Sci.* **2010,** *604*, 136-143.

(11). Ghazal Tofighi, X. Y., Henning Lichtenberg, Dmitry E. Doronkin, Wu Wang,

Christof Wöll, Yuemin Wang, and Jan-Dierk Grunwaldt. Chemical Nature of Microfluidically Synthesized AuPd Nanoalloys Supported on TiO_2. *ACS Catal.* **2019,** *9* (6), 5462-5473.

(12). Han, S.; Mullins, C. B. Surface Alloy Composition Controlled O_2 Activation on Pd–Au Bimetallic Model Catalysts. *ACS Catal.* **2018,** *8* (4), 3641-3649.

(13). Freakley, S. J.; He, Q.; Harrhy, J. H.; Lu, L.; Crole, D. A.; Morgan, D. J.; Ntainjua, E. N.; Edwards, J. K.; Carley, A. F.; Borisevich, A. Y.; Kiely, C. J.; Hutchings, G. J. Palladium-tin Catalysts for the Direct Synthesis of H_2O_2 with High Selectivity. *Science* **2016,** *351* (6276), 965-968.

(14) Savara, A.; Chan-Thaw, C. E.; Sutton, J. E.; Wang, D.; Prati, L.; Villa, A. Molecular Origin of Selectivity Differences Between Pd and AuPd in Benzyl Alcohol Oxidation: Different Oxygen Adsorption Properties. *ChemCatChem* **2017**, 2, 253-260.

(15). Hilaire, L. L. g., P.; Holl, Y.; Maire, G. Interaction of Oxygen and Hydrogen with Pd-Au Alloys: An AES and XPS Study. *Surf. Sci.* **1981,** *103*, 125-140.

(16). Adria R. Wilson, K. S., Miaofang Chi, Ryan M. White, James M. LeBeau, H. Henry Lamb and Benjamin J. Wiley. From Core−Shell to Alloys: The Preparation and Characterization of Solution-Synthesized AuPd Nanoparticle Catalysts. *J. Phys. Chem. C* **2013,** *117*, 17557-17566.

(17). Fu, Q.; Yang, Fan.; Bao, Xinhe.; Interface-Confined Oxide Nanostructures for Catalytic Oxidation Reactions. *Accounts Chem. Res.* **2013,** *46*, , 1169-1701.

(18). Huda, M.; Minamisawa, K.; Tsukamoto, T.; Tanabe, M.; Yamamoto, K. Aerobic Toluene Oxidation Catalyzed by Subnano Metal Particles. *Angew. Chem. Int.*

Edit. **2019,** *58* (4), 1002-1006.

(19). Vinod Kumar Puthiyapura, D. J. L. B., Andrea E. Russe, Wen-Feng Lin and Christopher Hardacre. Biobutanol as Fuel for Direct Alcohol Fuel Cells Investigation of Sn-Modified Pt Catalyst for Butanol Electro-oxidation. *ACS Appl. Mater. Inter.* **2016,** *8*, 12859-12870.

(20). Bai, X.; Chen, W.; Zhao, C.; Li, S.; Song,Y.; Ge, R.; Wei, W.; Sun, Y. Exclusive Formation of Formic Acid from CO_2 Electroreduction by Tunable Pd-Sn Alloy. *Angew. Chem. Int. Edit.* **2017,** *56* (40), 12219-12223.

(21). Clarke, J. Selectivity in Catalysis by Alloys. *Chem. Rev.* **1975,** *75* (3), 291-305.

(22). Vicente, A.; Lafaye, G.; Especel, C.; Marécot, P.; Williams, C. T. The Relationship Between the Structural Properties of Bimetallic Pd–Sn/SiO_2 Catalysts and Their Performance for Selective Citral Hydrogenation. *J. Catal.* **2011,** *283* (2), 133-142.

(23). Xu, J.; Wang, Y.; Cao, Y.; He, Z.; Zhao, L.; Etim, U. J.; Bai, P.; Yan, Z.; Wu, P. What is the Effect of Sn and Mo Oxides on Gold Catalysts for Selective Oxidation of Benzyl Alcohol? *New J. Chem.* **2019,** *43* (6), 2591-2599.

(24). Delley, B. An All-electron Numerical Method for Solving the Local Density Functional for Polyatomic Molecules. *J. Chem. Phys.* **1990,** *92* (1), 508-517.

(25). Delley, B. Fast Calculation of Electrostatics in Crystals and Large Molecules. *J. Phys. Chem.* **1996,** *100* (15), 6107-6110.

(26). Perdew, J. P.; Burke, K.; Ernzerhof, M. Generalized Gradient Approximation

Made Simple. *Phys. Rev. Lett.* **1996,** *77* (18), 3865-3868.

(27). Grimme, S. Semiempirical GGA-type Density Functional Constructed with a Long-range Dispersion Correction. *J. Comput. Chem.* **2006,** *27* (15), 1787-1799.

(28). Zhao, L. G., S.; Liu, H.; Zhu, H.; Yuan, S.; Guo, W. Density Functional Study of Hydrogen Evolution on Cobalt-Embedded Carbon Nanotubes: Effects of Doping and Surface Curvature. *ACS Appl. Nano Mater.* **2018,** *1*, 6258-6268.

(29). Halgren, T. A.; Lipscomb, W. N. The Synchronous-transit Method for Determining Reaction Pathways and Locating Molecular Transition States. *Chem. Phys. Lett.* **1977,** *49* (2), 225-232.

(30). Alwan, A. M.; Hashim, D. A.; Jawad, M. F. Efficient Modified Bimetallic Alloy Nanoparticles Porous Silicon Gas Sensors for CO Gas Detection Process. *Solid-State Electron.* **2019,** 153, 37-45.

(31). Dong, Q.; Wu, M.; Mei, D.; Shao, Y.; Wang, Y.; Liu, J.; Li, H.; Hong, L. Multifunctional Pd-Sn Electrocatalysts Enabled by In-situ Formed SnO_x and TiC Triple Junctions. *Nano Energy* **2018,** *53*, 940-948.

(32). Tsud, N.; Johanek, V.; Stara, I.; Veltruská, K.; Matolın, V. XPS, ISS and TPD Study of Pd–Sn Interactions on Pd–SnO_x Systems. *Thin Solid Films* **2001,** *391* (2), 204-208.

(33). Pushkarev, A. S.; Pushkareva, I. V.; Ivanova, N. A.; du Preez, S. P.; Bessarabov, D.; Chumakov, R. G.; Stankevich, V. G.; Fateev, V. N.; Evdokimov, A. A.; Grigoriev, S. A. Pt/C and Pt/SnO_x/C Catalysts for Ethanol Electrooxidation: Rotating Disk Electrode Study. *Catalysts* **2019,** *9* (3), 271.

(34). Wu, P.; Huang, Y.; Kang, L.; Wu, M.; Wang, Y. Multisource Synergistic Electrocatalytic Oxidation Effect of Strongly Coupled PdM (M= Sn, Pb)/N-doped Graphene Nanocomposite on Small Organic Molecules. *Sci. Rep.* **2015,** *5* (1), 14173.

(35). Elnaggar, M. E.; Shaheen, T. I.; Fouda, M. M.; Hebeish, A. A. Eco-friendly Microwave-assisted Green and Rapid Synthesis of Well-stabilized Gold and Core-shell Silver-gold Nanoparticles. *Carbohyd. Polym.* **2016,** *136*, 1128-1136.

(36). Tiruvalam, R.; Pritchard, J.; Dimitratos, N.; Lopez-Sanchez, J.; Edwards, J.; Carley, A.; Hutchings, G.; Kiely, C. Aberration Corrected Analytical Electron Microscopy Studies of Sol-immobilized Au+Pd, Au {Pd} and Pd {Au} Catalysts Used for Benzyl Alcohol Oxidation and Hydrogen Peroxide Production. *Faraday Discuss.* **2011,** *152*, 63-86.

(37). Silva, T. A. G.; Teixeira-Neto, E.; Lopez, N.; Rossi, L. M., Volcano-like Behavior of Au-Pd Core-shell Nanoparticles in the Selective Oxidation of Alcohols. *Sci. Rep.* **2014,** 4, 5766-5771.

(38). Kruse, N. XPS Characterization of Au/TiO_2 Catalysts: Binding Energy Assessment and Irradiation Effects. *Appl. Catal. A-Gen.* **2011,** *391* (1), 367-376.

(39). Wang, T.; Yuan, X.; Li, S.; Zeng, L.; Gong, J. CeO_2-modified Au@ SBA-15 Nanocatalysts for Liquid-phase Selective Oxidation of Benzyl Alcohol. *Nanoscale* **2015,** *7* (17), 7593-7602.

(40). Arrii, S.; Morfin, F.; Renouprez, A. J.; Rousset, J. L. Oxidation of CO on Gold Supported Catalysts Prepared by Laser Vaporization: Direct Evidence of Support Contribution. *J. Am. Chem. Soc.* **2004,** *126* (4), 1199.

(41). Liu, N.; Xu, M.; Yang, Y.; Zhang, S.; Zhang, J.; Wang, W.; Zheng, L.; Hong, S.; Wei, M. $Au^{\delta-}$–O_v–Ti^{3+} Interfacial Site: Catalytic Active Center toward Low-Temperature Water Gas Shift Reaction. *ACS Catal.* **2019,** *9* (4), 2707-2717.

(42). Mohammad, M.; Nishimura, S.; Ebitani, K. In Selective Aerobic Oxidation of 1, 3-propanediol to 3-hydroxypropanoic Acid Using Hydrotalcite Supported Bimetallic Gold Nanoparticle Catalyst in Water. AIP Conference Proceedings. American Institute of Physics **2015,** 1649(1), 58-66.

(43). Brun, M.; Berthet, A.; Bertolini, J. C. XPS, AES and Auger Parameter of Pd and PdO. *J. Electron Spectrosc.* **1999,** *104* (1–3), 55-60.

(44). Cao, X.; Cao, L.; Yao, W.; Ye, X. Structural Characterization of Pd-doped SnO_2 Thin Films Using XPS. *Surf. Interface Anal.* **1996,** *24* (9), 662-666.

(45). Gabasch, H.; Unterberger, W.; Hayek, K.; Klötzer, B.; Kleimenov, E.; Teschner, D.; Zafeiratos, S.; Hävecker, M.; Knop-Gericke, A.; Schlögl, R. In situ XPS Study of Pd(1 1 1) Oxidation at Elevated Pressure, Part 2: Palladium Oxidation in the 10^{-1} mbar Range. *Surf. Sci.* **2006,** *600* (15), 2980-2989.

(46). Wang, P.; Yuan, T.; Yuan, H.; Zheng, X.; Ijaz, H.; Hui, J.; Fan, D.; Zhao, Y.; Hu, S. PdO/SnO_2 Heterostructure for Low-temperature Detection of CO with Fast Response and Recovery. *RSC Adv.* **2019,** *9* (40), 22875-22882.

(47). Priolkar, K. R.; Bera, P.; Sarode, P. R.; Hegde, M. S.; Emura, S.; Kumashiro, R.; Lalla, N. P. Formation of $Ce_{1-x}Pd_xO_{2-\delta}$ Solid Solution in Combustion-Synthesized Pd/CeO_2 Catalyst: XRD, XPS, and EXAFS Investigation. *Chem. Mater.* **2002,** *14* (5), 2120-2128.

(48). Liu, C.; Kuang, Q.; Xie, Z.; Zheng, L. The Effect of Noble Metal (Au, Pd and Pt) Nanoparticles on the Gas Sensing Performance of SnO_2-based Sensors: A Case Study on the {221} High-index Faceted SnO_2 Octahedra. *CrystEngComm* **2015,** *17* (33), 6308-6313.

(49). Chen, Y.; Wang, H.; Liu, C. J.; Zeng, Z.; Zhang, H.; Zhou, C.; Jia, X.; Yang, Y. Formation of Monometallic Au and Pd and Bimetallic Au–Pd Nanoparticles Confined in Mesopores via Ar Glow-discharge Plasma Reduction and Their Catalytic Applications in Aerobic Oxidation of Benzyl Alcohol. *J. Catal.* **2012,** *289*, 105-117.

(50). Li, L.; Zhang, N.; He, H.; Zhang, G.; Song, L.; Qiu, W. Shape-controlled Synthesis of Pd Nanocrystals with Exposed {110} Facets and Their Catalytic Applications. *Catal. Today* **2019,** *327*, 28-36.

(51). Agostini, G.; Lamberti, C.; Pellegrini, R.; Leofanti, G.; Giannici, F.; Longo, A.; Groppo, E. Effect of Pre-reduction on the Properties and the Catalytic Activity of Pd/carbon Catalysts: A Comparison with Pd/Al_2O_3. *ACS Catal.* **2014,** *4* (1), 187-194.

(52). Wu, Y.; Tan, L.; Zhang, T.; Xie, H.; Yang, G.; Tsubaki, N.; Chen, J. Effect of Preparation Method on ZrO_2-based Catalysts Performance for Isobutanol Synthesis from Syngas. *Catalysts* **2019,** *9* (9), 752.

(53). Takashi Fujita, T. I., Kohei Shibamoto, Tetsuo Honma, Hironori Ohashi, Toru Murayama, and Masatake Haruta. CO Oxidation over Au/ZnO: Unprecedented Change of the Reaction Mechanism at Low Temperature Caused by a Different O_2 Activation Process. *ACS Catal.* **2019,** *9* (9), 8364-8372.

(54). Wang, H.; Liu, C.-j. Preparation and Characterization of SBA-15 Supported

Pd Catalyst for CO Oxidation. *Appl. Catal. B-Environ.* **2011,** *106* (3-4), 672-680.

(55). Dai, Q.; Zhu, Q.; Lou, Y.; Wang, X. Role of Brønsted Acid Site During Catalytic Combustion of Methane Over PdO/ZSM-5: Dominant or Negligible? *J. Catal.* **2018,** *357*, 29-40.

(56). Yu, W.; Mullen, G. M.; Mullins, C. B. Hydrogen Adsorption and Absorption with Pd–Au Bimetallic Surfaces. *J. Phys. Chem. C* **2013,** *117* (38), 19535-19543.

(57). Yang, G.; Frenkel, A. I.; Su, D.; Teng, X. Enhanced Electrokinetics of C-C Bond Splitting During Ethanol Oxidation by Using a Pt/Rh/Sn Catalyst with a Partially Oxidized Pt and Rh Core and a SnO_2 Shell. *ChemCatChem* **2016,** *8* (18), 2876-2880.

(58) Wu, P.; Liu, H.; Cao, Y.; Xi, S.; Li, Z.; He, Z.; Song, L.; Xu, J.; Bai, P.; Zhao, L.; Mintova, S.; Yan, Z. Mesostructured Cellular Foam Silica Supported Au–Pt Nanoalloy: Enrichment of D-state Electrons for Promoting the Catalytic Synergy. *Micropor. Mesopor. Mat.*, **2021**, 316, 110982.

(59) Savara, A.; Chan-Thaw, C. E.; Rossetti, I.; Villa, A.; Prati, L.; Benzyl Alcohol Oxidation on Carbon-Supported Pd Nanoparticles: Elucidating the Reaction Mechanism. *ChemCatChem* **2014**, 6, 3464–3473.

(60) Savara, A.; Rossetti, I.; Chan-Thaw, C. E.; Prati, L.; Villa, A. Microkinetic Modeling of Benzyl Alcohol Oxidation on Carbon-Supported Palladium Nanoparticles *ChemCatChem* **2016**, 8, 1–11.

For Table of Content use only

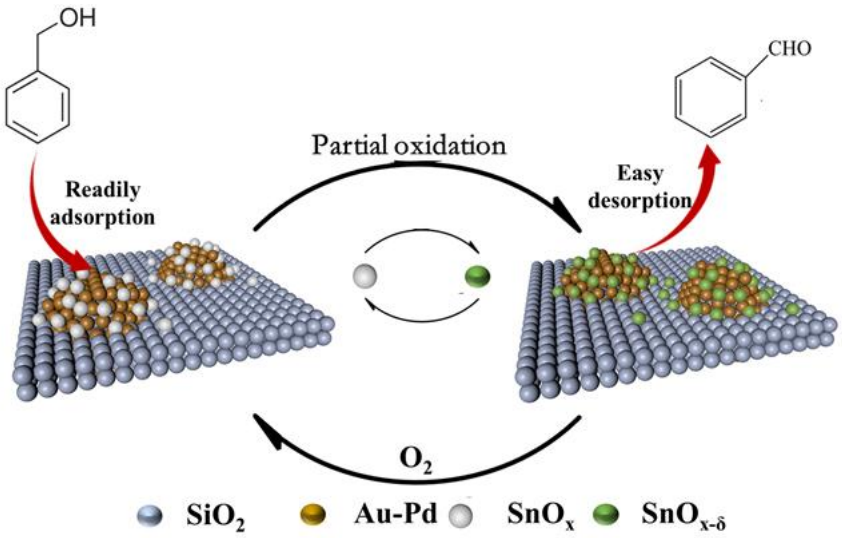
OH
CHO
Partial oxidation
Readily adsorption
Easy desorption
O2
SiO2
Au-Pd
SnOx
SnOx-δ